Title

Differential Excitability of PV and SST Neurons Results in Distinct Functional Roles in Inhibition Stabilization of Up States.

Journal

Journal of Neuroscience, 41(34)

ISSN

0270-6474

Authors

Romero-Sosa, Juan L
Motanis, Helen
Buonomano, Dean V

Publication Date

2021-08-25

DOI

10.1523/jneurosci.2830-20.2021

Peer reviewed

Systems/Circuits

Differential Excitability of PV and SST Neurons Results in Distinct Functional Roles in Inhibition Stabilization of Up States

Juan L. Romero-Sosa,[1,2] **Helen Motanis,**[1,3] **and Dean V. Buonomano**[1,2]

[1]Department of Neurobiology, Integrative Center for Learning and Memory, University of California, Los Angeles, Los Angeles, California 90095, [2]Department of Psychology, University of California, Los Angeles, Los Angeles, California 90095, and [3]Department of Neurosurgery, University of California, Los Angeles, Los Angeles, California 90095

Up states are the best studied example of an emergent neural dynamic regime. Computational models based on a single class of inhibitory neurons indicate that Up states reflect bistable dynamic systems in which positive feedback is stabilized by strong inhibition and predict a paradoxical effect in which increased drive to inhibitory neurons results in decreased inhibitory activity. To date, however, computational models have not incorporated empirically defined properties of parvalbumin (PV) and somatostatin (SST) neurons. Here we first experimentally characterized the frequency–current (*F–I*) curves of pyramidal (Pyr), PV, and SST neurons from mice of either sex, and confirmed a sharp difference between the threshold and slopes of PV and SST neurons. The empirically defined *F–I* curves were incorporated into a three-population computational model that simulated the empirically derived firing rates of pyramidal, PV, and SST neurons. Simulations revealed that the intrinsic properties were sufficient to predict that PV neurons are primarily responsible for generating the nontrivial fixed points representing Up states. Simulations and analytical methods demonstrated that while the paradoxical effect is not obligatory in a model with two classes of inhibitory neurons, it is present in most regimes. Finally, experimental tests validated predictions of the model that the Pyr ↔ PV inhibitory loop is stronger than the Pyr ↔ SST loop.

Key words: **inhibition; neural dynamics; neural network model; PV; SST; Up states**

Significance Statement

Many cortical computations, such as working memory, rely on the local recurrent excitatory connections that define cortical circuit motifs. Up states are among the best studied examples of neural dynamic regimes that rely on recurrent excitatory excitation. However, this positive feedback must be held in check by inhibition. To address the relative contribution of PV and SST neurons, we characterized the intrinsic input–output differences between these classes of inhibitory neurons and, using experimental and theoretical methods, show that the higher threshold and gain of PV leads to a dominant role in network stabilization.

Introduction

Many neural computations emerge from the intrinsic dynamics generated by the recurrent connectivity of neocortical microcircuits (Douglas and Martin, 2007; Rabinovich et al., 2008; Buonomano and Maass, 2009; Chaisangmongkon et al., 2017). Such intrinsically generated dynamic regimes are hypothesized to underlie a wide range of neural computations, including those in which the brain must temporarily store information (e.g., working memory) or produce appropriately timed responses in the absence of ongoing external inputs (Hebb, 1949; Hopfield, 1982; Wang, 2001; Mauk and Buonomano, 2004; Huertas et al., 2015). Indeed, *in vivo* studies have implicated internally generated dynamics in a range of memory and temporal computations (Quintana and Fuster, 1992; Funahashi et al., 1993; Shuler and Bear, 2006; Carnevale et al., 2015; Namboodiri et al., 2015; Guo et al., 2017; Inagaki et al., 2019). Some of these dynamic regimes, including self-sustained tonic and dynamically changing patterns of activity, have also been observed in *in vitro* and *ex vivo* circuits (Sanchez-Vives and McCormick, 2000; Wang, 2001; Johnson and Buonomano, 2007; Mann et al.,

Received Nov. 9, 2020; revised June 10, 2021; accepted June 13, 2021.

Author contributions: J.L.R.-S., H.M. and D.V.B. designed research; J.L.R.-S., H.M., and D.V.B. performed research; J.L.R.-S. and D.V.B. analyzed data; D.V.B. wrote the paper.

This work was supported by the National Institute of Mental Health grant MH60163 and supplement MH060163-15S1. We thank Rodrigo Laje and Saray Soldado-Magraner for comments on earlier versions of the manuscript. We also thank Carlos-Portera Cailliau, Peyman Golshani, Vishwa Goudar, Sotiris Masmanidis, and Michael Seay for helpful scientific discussions and technical assistance. In addition, we thank an anonymous reviewer for the suggestion to use the steady-state equations to establish the lower bound of the excitatory weights during searches.

The authors declare no competing financial interests.

Correspondence should be addressed to Dean V. Buonomano at dbuono@ucla.edu.

https://doi.org/10.1523/JNEUROSCI.2830-20.2021

2009; Sadovsky and MacLean, 2014; Carnevale et al., 2015; Carrillo-Reid et al., 2015; Dechery and MacLean, 2017), suggesting that the learning rules underlying internally generated neural dynamics are local and operational *ex vivo*.

The best studied form of emergent dynamics in neocortical circuits are Up states, a term that generally refers to network-wide regimes in which excitatory neurons can transition between quiescent Down states to more or less stable depolarized states with low to moderate firing rates (Sanchez-Vives and McCormick, 2000; Neske et al., 2015; Bartram et al., 2017). Up states can occur spontaneously or be evoked and are observed *in vivo* during anesthesia, slow-wave sleep, quiet wakefulness (Steriade et al., 1993; Timofeev et al., 2000; Beltramo et al., 2013; Hromádka et al., 2013), and acute slices (Sanchez-Vives and McCormick, 2000; Shu et al., 2003; Fanselow and Connors, 2010; Sippy and Yuste, 2013; Xu et al., 2013; Sadovsky and MacLean, 2014; Neske et al., 2015; Bartram et al., 2017), as well as in *ex vivo* cortical cultures (Plenz and Kitai, 1998; Seamans et al., 2003; Johnson and Buonomano, 2007; Kroener et al., 2009; Motanis and Buonomano, 2015, 2020). Up states have been proposed to have multiple functional roles, including memory consolidation and synaptic homeostasis (Tononi and Cirelli, 2003; Marshall et al., 2006; Sirota and Buzsáki, 2005; Vyazovskiy et al., 2008; Diekelmann and Born, 2010). It has also been hypothesized that Up states are equivalent to the desynchronized regimes of awake cortex (Destexhe et al., 2007). For example, the voltage distribution of Up states in awake cortex are indistinguishable from those observed during anesthesia (Constantinople and Bruno, 2011), and active sensory processing can shift cortical circuits to depolarized Up state-like patterns (Crochet and Petersen, 2006; Haider et al., 2007; Tan et al., 2014). The notion that Up states are related to active cortical processing regimes is further reinforced by theoretical studies in which Up states mirror so-called asynchronous regimes, wherein recurrently connected neurons are in a tonic, depolarized regime and spikes are triggered by ongoing fluctuations (Brunel, 2000; Renart et al., 2010; Tartaglia and Brunel, 2017). Together, these studies suggest that Up states reflect an important neural dynamic regime, and that neocortical circuits are programmed to seek out this regime under a wide range of conditions—including *in vivo* and *ex vivo* conditions.

Computational models have proposed that Up states reflect intrinsically generated dynamic regimes in which self-sustaining activity is maintained through positive feedback and is mediated through recurrent excitatory connections. This positive feedback is, in turn, held in check through rapid and strong inhibition, resulting in an inhibition-stabilized network (Tsodyks et al., 1997; Ozeki et al., 2009; Rubin et al., 2015; Jercog et al., 2017). To date, these models have effectively captured many aspects of Up-state/Down-state transitions and asynchronous network dynamics (Brunel, 2000; Holcman and Tsodyks, 2006; Renart et al., 2010; Dao Duc et al., 2015; Jercog et al., 2017; Tartaglia and Brunel, 2017). However, these models have focused primarily on a single unspecified class of inhibitory (*I*) neurons. Yet, it is well established that multiple classes of inhibitory neurons are active during Up states recorded *in vivo* and in acute slices (Neske et al., 2015; Urban-Ciecko et al., 2015; Neske and Connors, 2016; Zucca et al., 2017). Thus, the respective functional roles of these interneurons remain mostly unaddressed.

Here we use experimental and computational methods to study the role of the two most common populations of inhibitory neurons—parvalbumin (PV)-positive and somatostatin (SST)-positive neurons (Rudy et al., 2011)—in emergent dynamics. Experiments were performed in *ex vivo* organotypic cortical cultures to ensure that the experimental observations parallel our "stand-alone" computational model. Organotypic slices are a standard preparation to study synaptic plasticity and cortical microcircuit functions (Debanne et al., 1994; Hayashi et al., 2000; Esteban et al., 2003; Seamans et al., 2003; Kerr and Plenz, 2004; Goold and Nicoll, 2010; Yamada et al., 2010). *Ex vivo* organotypic slices provide a manner to unambiguously ascertain that the observed dynamics emerge locally within the circuit being studied. Additionally, consistent with the notion that Up states reflect a core dynamic regime that cortical circuits are programmed to seek out, spontaneous and evoked Up states emerge in cortical organotypic cultures over the course of *ex vivo* development (Johnson and Buonomano, 2007; Motanis and Buonomano, 2015, 2020). Overall, our approach allowed us to directly compare experimental and model parameters of PV and SST neurons. Surprisingly, they reveal that the intrinsic properties of PV and SST neurons are sufficient to predict robust differential contributions of these inhibitory neuron classes emergent dynamics.

Materials and Methods

Electrophysiology and ex vivo *slices.* All animal experiments followed guidelines established by the National Institutes of Health and were approved by the Chancellor's Animal Research Committee at the University of California, Los Angeles. Organotypic slices were prepared using the interface method (Stoppini et al., 1991; Buonomano, 2003). Five to 7-d-old PV-Cre and SST-Cre mice pups of either sex (catalog #017320 and #013044, respectively, The Jackson Laboratory) were anesthetized with isoflurane and decapitated. The brain was removed and placed in chilled cutting media. Coronal slices (400 μm thickness) containing primary somatosensory and auditory cortex were sliced using a vibratome (model VT1200, Leica) and placed on filters (MillicellCM, Millipore) with 1 ml of culture media. Culture media was changed at 1 and 24 h after cutting and every 2–3 d thereafter. Cutting media consisted of Eagle's minimal essential medium (EMEM; catalog #15–010, MediaTech) plus the following (final concentration in mM): 3 $MgCl_2$; 10 glucose; 25 HEPES; and 10 Tris-base. Culture media consisted of EMEM plus the following (final concentration in mM): 1 glutamine; 2.6 $CaCl_2$; 2.6 $MgSO_4$; 30 glucose; 30 HEPES; 0.5 ascorbic acid; 20% horse serum; 10 U/L penicillin; and 10 μg/L streptomycin. Slices were incubated in 5% CO_2 at 35°C.

Recordings were performed at 23–35 d *in vitro* (DIV) in artificial CSF (ACSF) composed of the following (in mM): 125 NaCl, 5.1 KCl, 2.6 $MgSO_4$, 26.1 $NaHCO_3$, 1 NaH_2PO_4, 25 glucose, and 2.6 $CaCl_2$ (ACSF was formulated to match the standard culture media). The temperature was maintained at 32–33°C, and the perfusion rate was set at 4.5–5 ml/min.

Recordings from pyramidal (Pyr) neurons relied on visualized whole-cell patching and were identified based on their intrinsic electrophysiological properties. Florescent PV and SST neurons were targeted using a 565 nm LED to visualize tdTomato. The internal solution for whole-cell recordings contained the following (in mM): 100 K-gluconate, 20 KCl, 4 ATP-Mg, 10 phospho-creatine, 0.03 GTP-Na, and 10 HEPES, adjusted to pH 7.3 and 300 mOsm. To be considered for analysis, cells had to have a resting potential of less than −55 mV and to not change by >15% over the course of the recording. The criteria for input and series resistance were 100–300 and <25 MΩ, respectively.

To estimate the average Up-state membrane potential during light stimulation and after light stimulation, the entire trace was filtered with a 10 ms median filter. Two 100-ms-long windows were isolated from the trace, one during light stimulation and the other 100 ms after the end of light stimulation. These windows were averaged to get one membrane potential value per neuron.

Transfection and optogenetics. PV-Cre and SST-Cre slices were transfected in the following three different configurations: (1) 2.2 µl of ChETA (pAAV9-Ef1a-DIO-ChETA-EYFP; catalog #26968, Addgene) and 1 µl of LSL-tdTomato (catalog #100048, Addgene); (2) 2.2 µl of DIO eNpHR 3.0 and 1 µl of LSL-tdTomato; or (3) 1 µl of LSL-tdTomato. The approximate titer of all viral solutions was 1×10^{13} viral genomes/ml. Note that some of the paired recording data was obtained in slices transfected with halorhodopsin as part of other experiments. Transfection was performed at 5–7 DIV by gently delivering the virus mixture in a patch electrode at three to five positions in the cortex of the slice to transfect as many Cre-positive cells as possible. Experiments were performed at least 16–18 d after transfection.

Light stimulation was performed in a closed-loop fashion. A custom-written Signal script (Cambridge Electronic Design) detected threshold crossings (~5 mV) that marked the potential onset of an Up state, which triggered light stimulation after a delay of 250 ms. Light stimulation consisted of either 15 pulses at 66 Hz (5 ms on) or 25 pulses at 50 Hz (10 ms on). Light stimulation was delivered via a royal blue (457 nm) LED (SuperBright LEDs) at an intensity of 78 mW/cm^2.

Statistics. Nonrepeated one-way ANOVAs were performed in MATLAB. The Up-state duration and voltage (see Fig. 8) were not normally distributed (*kstest* in MATLAB); thus, we used paired nonparametric statistics to contrast these measures (*signrank* in MATLAB).

Computational model. Our three-population model was based on the two-population model of Jercog et al. (2017). The model was composed of three classes of neurons representing the excitatory pyramidal neurons (*E*), PV neurons (*P*), and SST (*S*). Each of these populations was modeled as a single "unit" according to the following:

$$\tau_E \frac{dE}{dt} = -E(t) + f_E\big(W_{EE}E(t) - W_{EP}P(t) - W_{ES}S(t) + \eta_E(t)\big) \quad (1)$$

$$\tau_P \frac{dP}{dt} = -P(t) + f_P\big(W_{PE}E(t) - W_{PP}P(t) - W_{PS}S(t) + \eta_P(t)\big) \quad (2)$$

$$\tau_S \frac{dS}{dt} = -S(t) + f_S\big(W_{SE}E(t) - W_{SP}P(t) - W_{SS}S(t) + \eta_S(t)\big), \quad (3)$$

where W_{XY} represents the weight between the postsynaptic unit X (*E*, *P*, or *S*) and presynaptic unit Y (*E*, *P*, or *S*). τ_X and η_X represent a time constant and an independent noise term, respectively. Similar to Jercog et al. (2017), the noise term was an Ornstein–Uhlenbeck process with a time constant of 1 ms and an SD of σ_X. We did not include an adaptation term that contributes to Up → Down transitions because we focused primarily on steady-state values. Thus, all the Up → Down and Down → Up transitions shown in the figures were fluctuation induced. Because all analyses focused on fixed-point Up-state values, the results presented are independent of Up ↔ Down transitions. The function $f_Y(x)$ represents the intrinsic excitability of the three neuron classes (i.e., the frequency–current (*F–I*) curve or activation function), which were simulated as a threshold-linear function characterized by a threshold (θ_X) and a gain that corresponds to the slope of the *F–I* curve (g_X), as follows:

$$f_Y(x) = \begin{cases} 0 \text{ if } x < \theta_Y \\ f_Y(x)g_Y \text{ if } x \geq \theta_Y \end{cases}, Y = \{\{E, P, S\}. \quad (4)$$

Paradoxical effect. To examine the paradoxical effect, we stimulated the *P* or *S* neurons by emulating an optogenetic experiment. Mathematically, an external current is equivalent to decreasing the threshold of the *F–I* function (Eq. 4). Specifically, the threshold in the presence of simulated light activation can be written as $\theta_X^L = \theta_X - L_X$, where the subscript X represents the *P* or *S* population, and L_X captures the optogenetic activation of either population (L_X = 5 and 20 for the weak and strong activation, respectively).

Empirical fits of the F–I *functions.* During whole-cell recordings, intrinsic excitability was measured with 250 ms current steps in the range of 0.05–0.6 nA, depending on cell class. For each neuronal class, we fit the mean spike *F–I* curve to a threshold-linear activation function (Eq. 4), which led to threshold values of 0.06, 0.36, and 0.18 nA, and gains of 124, 334, and 198 Hz/nA, for the Pyr, PV, and SST neuron classes, respectively. To simplify the units and to maintain the weight magnitudes used in the study by Jercog et al. (2017), we normalized the observed θ and g to those of the excitatory unit used by Jercog et al. (2017), (θ_E = 5, g_E = 1). For example, θ_E was set to 5, leading to θ_P = 5*0.36/0.06 = 30. Thus, the intrinsic excitability values for the threshold, θ_X, were 5, 30, and 15, and the gain values, g_X, were 1, 2.7, and 1.6 for the *E*, *P*, and *S*, populations, respectively.

We also set the values of τ_X to the fits of the mean membrane time constants of the Pyr, PV, and SST neurons (10, 4, and 6 ms for *E*, *P*, and *S*, respectively). We note, however, that the time constant in Equations 1–3 is often interpreted as corresponding to the synaptic time constant (Shriki et al., 2003; Ozeki et al., 2009) rather than the membrane time constants. However, this interpretation is less parsimonious with the current formulation in which the IPSCs from PV and SST cells can have different time constants.

Fitting model weights to the empirically defined firing rates. To find the weights sets or vectors that captured the empirically observed mean firing rates of the Pyr, PV, and SST neurons, we performed a parameter search over the nine weight variables with empirically derived values of (i.e., θ_E, θ_P, θ_S, g_E, g_P, g_S, τ_E, τ_P, and τ_S). The search values were approximately centered on the values used by Jercog et al. (2017), as follows:

$$W_{EE} = [2 : 0.5 : 9]$$

$$W_{EP} = W_{ES} = [0 : 0.5 : 4]$$

$$W_{PE} = W_{SE} = [2 : 2 : 18]$$

$$W_{PP} = W_{SS} = W_{PS} = W_{SP} = [0 : 1 : 5].$$

The bracketed values represent the minimum, step size, and maximal values of the corresponding weight search. We searched a parameter space of 15 × 9 × 9 × 9 × 9 × 6 × 6 × 6 × 6 for a total of 127,545,840 parameter sets. The lower search bound for W_{EE} was based on Equation 1 when all inhibitory weights were 0 and *E* at its set point (i.e., the lowest W_{EE} value that could generate the target firing rate is the value unchecked by any inhibition). Similarly, the lower bounds for W_{PE} and W_{SE} can be calculated in the same way. Interestingly, this calculation already reveals that the lower bound of W_{PE} is larger than that of W_{SE} as a result of $\theta_P > \theta_S$. This observation is consistent with the overall conclusion that inhibition stabilization is more reliant on PV neurons than SST neurons. However, to provide an unbiased search in which all *P*- and *S*-related weights were searched over the same values, we used the W_{SE} as the lower bound for both W_{PE} and W_{SE}.

For each weight vector, we ran the simulation for 1.5 s (dt = 0.1 ms) and defined the steady-state values of each population as the mean firing rate over the last 100 ms. Since the goal of the search was to find weight sets that produced Up-state firing rates that matched the experimental data, these simulations were run in the absence of noise to prevent spontaneous Up → Down transitions. To induce evoked Down → Up transitions, an input pulse of 25 ms and an amplitude of 7 were applied to the *E* units at 500 ms.

We defined the accepted group of weight sets as those that led to fits in which all three Up-state firing rates (i.e., steady-state *E*, *P*, and *S* values) were within ±25% of the empirically observed rates (5, 14, and 17 Hz, for the Pyr, PV, and SST populations, respectively)—note that to satisfy this criterion the firing rates had to be stable fixed points (i.e., nonoscillatory). The criterion of ±25% was used because it allowed larger step sizes in the weight parameter search (helping constrain the number of searched weight vectors). Furthermore, the range captures the experimentally observed variability in Up-state firing rates.

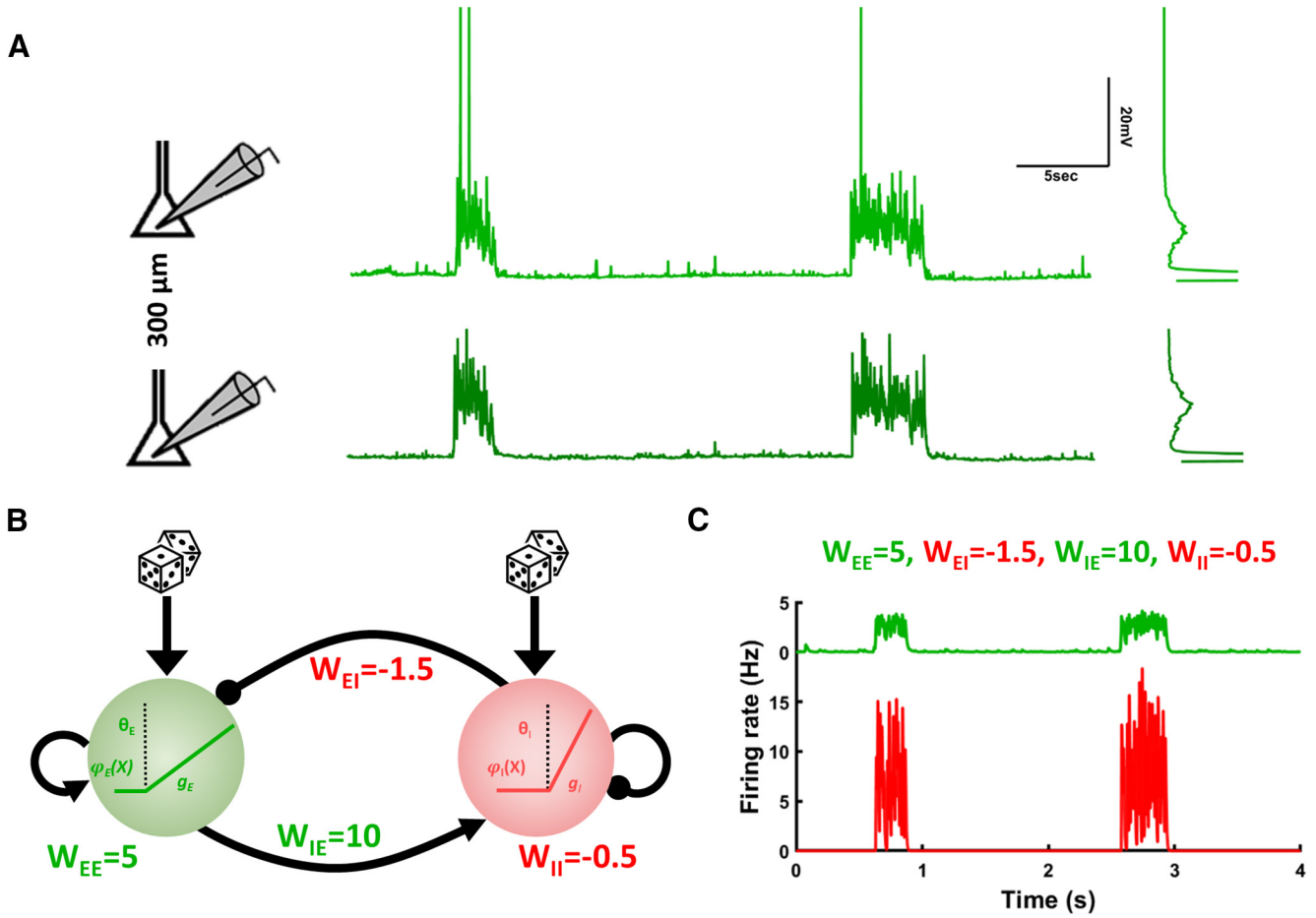

Figure 1. Experimental Up states and numerical simulations in a two-population model. ***A***, Example of Up states recorded in an *ex vivo* cortical circuit. Traces represent two simultaneously recorded pyramidal neurons separated by ~300 µm. Insets to the right show the bimodal distribution of membrane voltage (the peak of the distribution, which is centered at rest, is clipped for visualization purposes). ***B***, Schematic of the two-population model with an excitatory (green) and inhibitory (red) population. Each population is simulated by a linear threshold activation function defined by threshold (q), and gain (g). Lines with arrows represent excitatory connections, and lines with dots represent inhibitory connections. Dice represents noise. ***C***, Example of simulated Up states in the E (top trace) and I populations (bottom trace) from the model with the indicated weight values.

Analysis of fixed points and the paradoxical effect. To derive the Up-state fixed points for all three populations (E^*, P^*, and S^*) of Equations 1–3 in the linear regime (i.e., E, P, and $S > 0$), we can first impose that all three derivatives be equal to 0 and obtain the following:

$$g_E\theta_E = -E + W_{EE}g_E E - W_{EP}g_E P - W_{ES}g_E S \quad (5)$$

$$g_P\theta_P = -P + W_{PE}g_P E - W_{PP}g_P P - W_{PS}g_P S \quad (6)$$

$$g_S\theta_S = -P + W_{SE}g_S E - W_{SP}g_S P - W_{SS}g_S S. \quad (7)$$

By solving this set of equations, and through multiple substitution steps, it can be shown that the Up state fixed point of P is as follows:

$$P^* = \frac{\theta_P\left(W'_{SS}*W'_{EE} - W_{ES}*W_{SE}\right) + \theta_E\left(W_{PS}*W_{SE} - W_{PE}*W'_{SS}\right) + \theta_S\left(W_{ES}*W_{PE} - W_{PS}*W'_{EE}\right)}{W_{EP}*W_{PE}*W'_{SS} - W'_{EE}*W'_{PP}*W'_{SS} + W_{ES}*W_{SE}*W'_{PP} + W_{PS}*W_{SP}*W'_{EE} - W_{EP}*W_{PS}*W_{SE} - W_{ES}*W_{PE}*W_{SP}} \quad (8)$$

where $W'_{SS} = W_{SS} + \frac{1}{g_S}$, $W'_{PP} = W_{PP} + \frac{1}{g_P}$, and $W'_{EE} = W_{EE} - \frac{1}{g_E}$. Importantly, it is only the first term of the numerator that is critical to determining whether the paradoxical effect (in the P population) is present in response to P activation. Specifically, external tonic depolarization of the P population is equivalent to decreasing θ_P. Thus, we can see that such a decrease will lead to a decrease in P^* (i.e., the paradoxical effect) if $W'_{SS} * W'_{EE} > W_{ES} * W_{SE}$, and to an increase in P^* if $W'_{SS} * W'_{EE} < W_{ES} * W_{SE}$. An equivalent equation can be derived for S^*. Note that this rationale assumes that the denominator is always positive for stable fixed points. While we did not formally establish that this was the case, we did verify that the denominator was indeed positive for all solutions obtained in our parameter search.

Data availability. The code used for the simulations is available at https://github.com/BuonoLab/RomeroSosaMotanisBuonomano_UpStates_2021.

Results

The two-population model of Up states

Up states are characterized by transitions from a quiescent network-wide Down state to a regime in which excitatory neurons

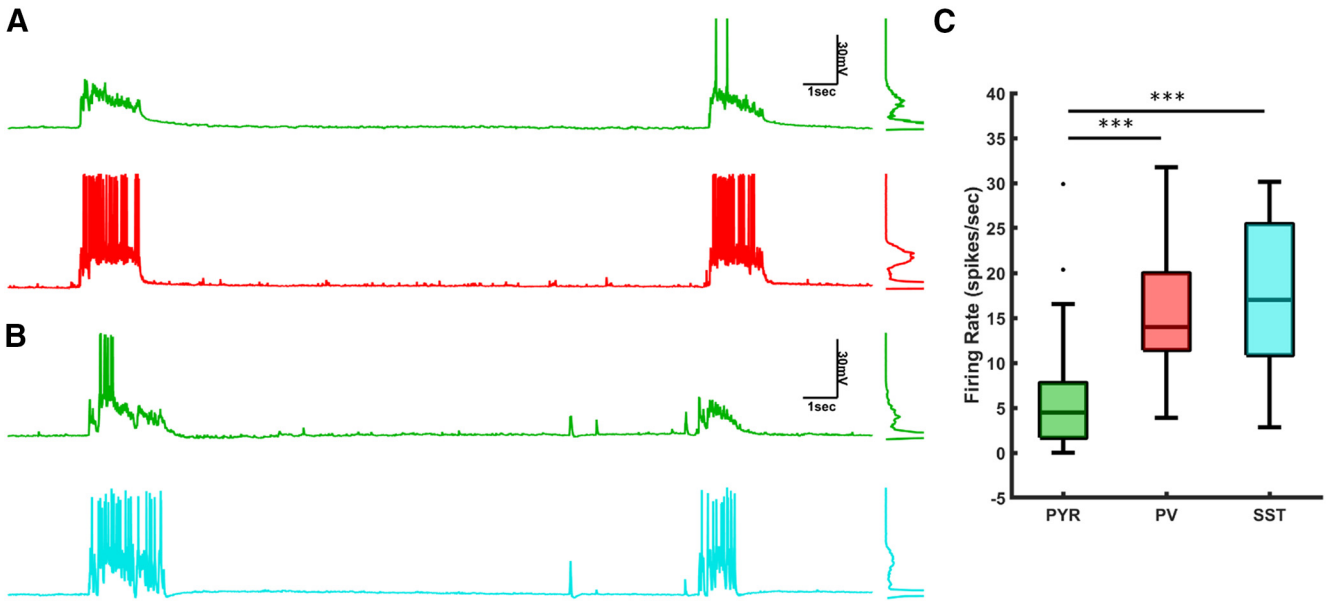

Figure 2. Experimentally observed Up-state signatures in Pyr, PV, and SST neurons. ***A***, Example of Up states in simultaneously recorded Pyr and PV neurons. ***B***, Example of Up states in simultaneously recorded Pyr and SST neurons. ***C***, Mean firing rate of Pyr, PV, and SST neurons during Up states.

are depolarized and fire at moderate rates. Figure 1*A* illustrates Up-Down transitions in two simultaneously recorded Pyr neurons in an *ex vivo* slice of the auditory cortex. Both neurons transition between Up and Down states simultaneously, and during Up states they maintain an approximately constant level of membrane depolarization, resulting in the characteristic bimodal distribution of membrane voltages (Mann et al., 2009; Lőrincz et al., 2015). Importantly, during Up states, the firing rate of pyramidal neurons is far below saturation, indicating that they do not reflect pathologic regimes characterized by saturated firing rates or paroxysmal discharges (Connors, 1984; Prince and Tseng, 1993; Timofeev et al., 2004).

The Up and Down states illustrated in Figure 1*A* have typically been interpreted to reflect bistable network regimes in which Down states correspond to a trivial fixed point where excitatory firing rates are approximately zero, and Up states correspond to a nontrivial fixed point with moderate firing rates. Computational studies have carefully characterized such regimes in firing rate and spiking neural network models (Brunel, 2000; Holcman and Tsodyks, 2006; Renart et al., 2010; Dao Duc et al., 2015; Jercog et al., 2017; Tartaglia and Brunel, 2017). Figure 1*B* shows an example of a firing rate model of Up states based on the study by Jercog et al. (2017; see Materials and Methods). The model is composed of variables representing the firing rates of a population of E and inhibitory I neurons connected through the synaptic weights: W_{EE} ($E \rightarrow E$), W_{EI} ($I \rightarrow E$), W_{IE} ($E \rightarrow I$), and W_{II} ($I \rightarrow I$). Intuitively, the Up-state and Down-state transitions in the model can be understood as a noisy excitatory input to the E population, which sometimes reaches threshold, and triggers positive feedback through the $E \rightarrow E$ connection. In parallel, the I population receives an increasing excitatory drive from E, triggering rapid and strong inhibition of the E unit—settling in an inhibition stabilized fixed-point attractor (Fig. 1C; Tsodyks et al., 1997; Ozeki et al., 2009; Jercog et al., 2017).

As with most Up-state models to date, this model incorporates only a single unspecified class of inhibitory neurons. However, it is well established that there are distinct populations of inhibitory neurons within the neocortex and that these neurons have distinct properties and functional roles in cortical computations (Adesnik et al., 2012; Kuhlman et al., 2013; Pi et al., 2013; Natan et al., 2017). Here we focused explicitly on PV and SST neurons as they are the most common types of inhibitory neurons (Rudy et al., 2011), and because VIP (vasoactive intestinal polypeptide) neurons have been associated with changes in brain states and cross-cortical interactions (Pi et al., 2013; Krabbe et al., 2019), which are not present in the *ex vivo* experimental preparation we are simulating.

Characterization of Pyr, PV, and SST neurons during Up states

To characterize the firing rates and intrinsic properties of PV and SST neurons, we recorded from *ex vivo* cortical slices of PV-Cre and SST-Cre animals that expressed the tdTomato marker in PV or SST neurons, respectively. Targeted paired whole-cell recordings of Pyr and PV or Pyr and SST were performed. Both PV and SST neurons transitioned between Up and Down states in near synchrony with Pyr neurons (Fig. 2*A*,*B*). PV and SST neurons exhibited firing rates significantly above those of the Pyr neurons (Fig. 2*C*; one-way ANOVA: $F_{(2,75)} = 20.3$, $p < 0.001$). The median firing rate of the three neuron classes was as follows: Pyr: 4.5, interquartile range (IQR) = 6.09 Hz ($n = 39$); PV: 14, IQR = 8.55 Hz ($n = 26$); and SST: 17, IQR = 14.58 Hz ($n = 13$; Wilcoxon signed-rank test: Pyr × PV, $z = -5.02$, $p < 0.001$; Pyr × SST, $z = -4.19$, $p < 0.001$). Interestingly, PV Up-state onset occurred earlier than Pyr Up-state onset, but this was not the case for SST Up states (Fig. 3).

To build a three-population model composed of an excitatory population and two inhibitory neuron populations, a critical issue is what are the defining differential characteristics between the two inhibitory neuron populations—typically, it has been assumed that what differentiates PV and SST neurons is their connectivity patterns (see Discussion). Here, as a first step toward building an empirically grounded three-population model of Up states, we measured the *F–I* function of Pyr, PV, and SST neurons and characterized their firing properties (Fig. 4*A*). A mixed two-way ANOVA (cell type × intensities range, 0.05–0.4 nA) revealed a significant cell-type factor ($F_{(2,77)} = 17.7$,

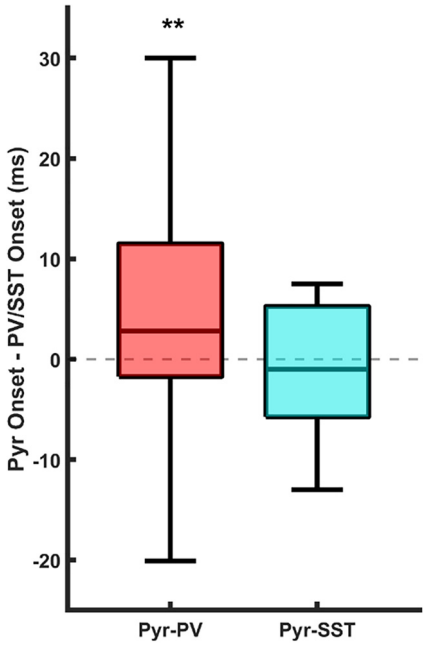

Figure 3. Onset times of Up state in PV and SST neurons relative to Pyr neurons. Relative to Up-state onset in Pyr neurons, Up-state onset in PV and SST neurons was defined as the threshold-crossing time (5 mV above rest) within a window of ±50 around Pyr Up-state onset. Relative to Pyr neurons, median onset times in PV and SST neurons were 2.8 ms ($p < 0.002$, t test) and −1 ms, respectively.

$p < 10^{-6}$). Pairwise comparisons revealed that PV F–I curves were significantly different from those in Pyr ($p < 10^{-6}$, Tukey–Kramer test) and SST ($p = 0.012$), and that there was no difference between Pyr and SST ($p = 0.1$).

We next fit the F–I curves to a rectified linear unit (ReLU) function, which was defined by two variables: a threshold (θ) and a slope (the gain g). The fitted threshold (θ_E) and gain (g_E) values of the Pyr neurons (θ_E = 0.06 nA, g_E = 124 Hz/nA) were below the threshold and gain values of the PV (θ_P = 0.36 nA, g_P = 334 Hz/nA) and SST (θ_S = 0.18 nA, g_S = 198 Hz/nA) neurons (Fig. 4*B*).

Empirically based Up-state model with Pyr, PV, and SST populations

To the best of our knowledge, the above results provide the first opportunity to directly simulate a three-population model based on empirically defined F–I curves and fit the weights of the model to match the observed firing rates in the three neuronal populations. We thus extended the model presented in Figure 1*B* to include the following three populations: Pyr (E), PV (P), and SST (S; Fig. 5*A*). While *in vitro* experiments from acute slices have revealed a significant amount of information about the interconnectivity among these three populations (Silberberg and Markram, 2007; Pfeffer et al., 2013; Xu et al., 2013), we chose to perform an unbiased assumption-free implementation of the model to directly determine the predictions generated by a model based on empirically derived F–I curves. Thus, we implemented a fully interconnected model with all nine connection classes (Fig. 5*A*; see Materials and Methods).

We performed an unbiased search to determine which sets of weights would generate the experimentally observed firing rates (see Materials and Methods). By an unbiased search, we mean that the parameter space was the same for all P- and S-related weights (e.g., the range of W_{EP} values explored was equal to the range of W_{ES} values). We explored ~127 million sets of weights. As there are nine weights and three firing rates to be fit, the parameter search is underconstrained, resulting in a distribution of weight sets that accounted for the experimentally observed firing rates. Of 127 million weight sets, 10,578 generated Up-state firing rates of all three cell types (i.e., steady-state E, P, and S values) that were within ±25% of the empirically observed rates. We refer to this as the set of fit weights (see Materials and Methods). Figure 5*B* shows spontaneous Up and Down states of the E, P, and S populations in a simulation run with the prototypical weight set—which we define as the weight vector closest to the centroid of all of the fit weight vectors.

To test the hypothesis that the empirically derived intrinsic properties of the PV and SST cells play a deterministic role in their functional contribution to Up states, we explored the relative distribution of weights of the P and S populations in the fit weight sets. Stability analyses have established that in the two-population model two conditions must be met for stability (Ozeki et al., 2009). One of these conditions can be thought of as requiring that the "net inhibition" be stronger than the "net excitation." Mathematically, this can be expressed $W_{EI} * W_{IE} > W'_{EE} * W'_{II}$ (where $W'_{EE} = W_{EE} - 1/g_E$ and $W'_{II} = W_{II} + 1/g_I$). Note that $W_{EI}W_{IE}$ reflects the strength of the net inhibitory loop in the two-population model, while $W'_{EE} * W'_{II}$ captures the net excitation as the weight of the inhibitory population onto itself (W_{II}) is functionally excitatory. Since the gains were constant throughout our search, the notion of net excitation and net inhibition suggests an intuitive way to distill the analyses of weight vectors that satisfied the search criteria. We thus first compared the distribution of the net inhibition minus the net excitation for the $E \leftrightarrow P$ and $E \leftrightarrow S$ loops. As shown in Figure 5, *C* and *D*, for the $E \leftrightarrow P$ loop, $W_{EP}W_{PE} > W_{EE}W_{PP}$ in 80% of the fit weight sets. In contrast, in the $E \leftrightarrow S$ loop only 8% of the fit weights were $W_{ES}W_{SE} > W_{EE}W_{SS}$. To directly contrast the contribution of P and S populations, we also examined the net P inhibition minus the net S inhibition: $W_{EP}W_{PE} - W_{ES}W_{SE}$. This contrast revealed that in 85% of the cases the net P inhibition was more robust than the net S inhibition (Fig. 5*E*). These results suggest that solely because of the intrinsic properties of the two inhibitory neuron classes, the P population generally emerges as the one primarily responsible for an inhibition stabilization. Nevertheless, in a minority of the parameter regimes, $W_{ES}W_{SE}$ was larger than $W_{EP}W_{PE}$; however, in most of these cases, W_{EP} or W_{PE} was close to or equal to zero. Thus, in the absence of a $P \leftrightarrow E$ loop, the intrinsic properties of the S neurons form a "backup" system that can support Up states and fulfill the role of inhibition stabilization.

The paradoxical effect

The above results predict that the net inhibition in the $E \leftrightarrow P$ loop is stronger than in the $E \leftrightarrow S$ loop. But, interestingly, this observation does not translate into meaning that PV neurons are more effective at modulating Up states (e.g., turning Up states off). In part precisely because of the strength of the $E \leftrightarrow P$ loop, changes in the external input to P engage a dynamic rebalancing of excitation and inhibition resulting in counterintuitive properties, including the so-called "paradoxical effect" that has been described in the two-population model (Tsodyks et al., 1997; Rubin et al., 2015). Specifically, in the two-population model (Fig. 1*B*), if the I unit is artificially activated during an Up state, an overall decrease in I activity is observed. This is because

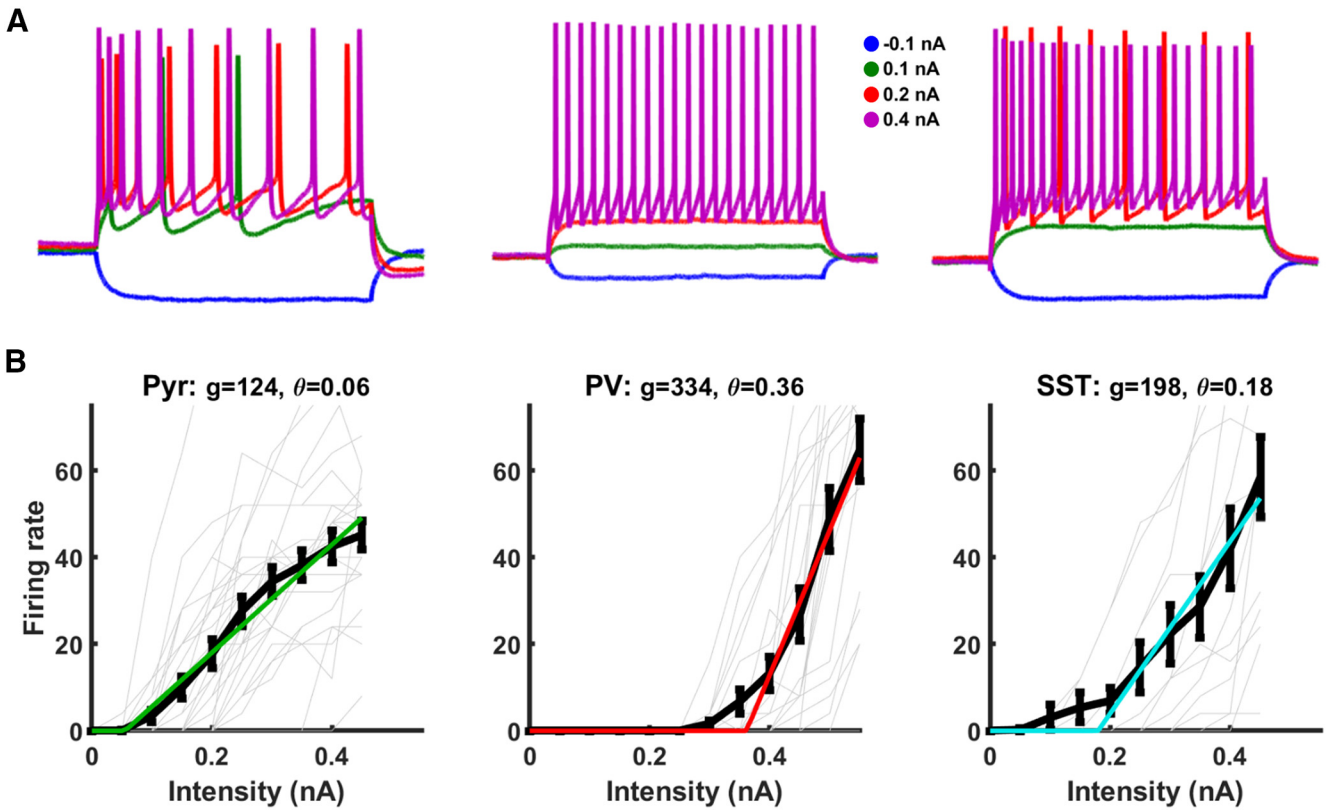

Figure 4. *F–I* curve fits of the intrinsic excitability of Pyr, PV, and SST neurons. ***A***, Top, Sample intrinsic excitability of Pyr (left), PV(middle), and SST(right) neurons in response to depolarizing current steps of −0.1, 0.1, 0.2, and 0.4 nA. ***B***, Threshold-linear fits of the *F–I* curves of Pyr populations. Light gray lines are the *F–I* curves of individual neurons. Black lines are the mean plus SEs of the *F–I* curves, and colored lines are the fits. The gain ($g_P = 334$) and the threshold ($q_P = 0.36$) of PV (middle) neurons is higher than in Pyr neurons ($g_E = 124$, $q_E = 0.06$; left) and SST neurons ($g_S = 198$, $q_S = 0.18$; right).

increasing *I* decreases *E*, which in turn decreases excitatory drive to *I*. The net result is that for *E* to settle at a lower fixed point, *I* must also settle at a lower fixed point (to maintain an *E*/*I* balance). In the two-population model, this paradoxical effect is obligatory (Tsodyks et al., 1997; Jercog et al., 2017). Thus, we next examined the properties of the paradoxical effect in the three-population model and whether *P* or *S* activation is more effective at turning off Up states (Fig. 6*A*). In a model with the prototypical weights, weak *P* activation during an Up state (see Materials and Methods) produced a paradoxical effect. In contrast, weak *S* stimulation did not result in a paradoxical effect (i.e., there was an increase in steady-state *S* activity after external *S* activation; Fig. 6*A*, middle). Across the ~10,000 weight sets that fit the data, the paradoxical effect was observed in 96% and 18% of cases in the *P* and *S* units, respectively (Fig. 6*A*, bottom).

Counterintuitively, although the $E \leftrightarrow P$ inhibitory loop was stronger than the $E \leftrightarrow S$ loop, weak activation of *S* units was more likely to induce an Up → Down transition (3.7%) than weak activation of *P* units (0.6%; Fig. 6*A*, bottom). But, as expected, strong depolarization of *P* or *S* (Fig. 6B) units was likely to induce Up → Down transitions, and now *P* activation was more effective at turning off Up states (84%) than *S* activation (23%; Fig. 6*B*, bottom).

In the vast majority of the fit weight vectors, the paradoxical effect was observed in either the *P* or *S* units in response to *P* or *S* stimulation, respectively. Interestingly, however, there was a very small number of weight sets (0.4%) in which the paradoxical effect was not observed in either the *P* or *S* population (Fig. 6*C*). This observation has important experimental implications as it establishes that although the paradoxical effect is expected in most parameter regimes, it is not obligatory in a model with two types of inhibitory neurons—a potentially relevant observation because a number of experimental studies have failed to observe the paradoxical effect (Xu et al., 2013; Gutnisky et al., 2017; see Discussion).

Analysis of the steady-state equations confirmed the numerical simulations (see Materials and Methods) and showed that whether or not the paradoxical effect is present in the *P* population, for example, depends on the coupling between the *E* and *S* populations. Specifically, if $W'_{SS} * W'_{EE} \geq W_{ES} * W_{SE}$ (i.e., if excitation is stronger than inhibition in the $E \leftrightarrow S$ loop; see Materials and Methods) the paradoxical effect will be observed in the *P* population. Indeed, we can see that if W_{ES} or W_{SE} is equal to zero, the network is effectively equivalent to the two-population model, in which case the paradoxical effect must be present in the *P* population. In contrast, if $W_{ES} * W_{SE}$ is relatively high (strong *S* inhibition), then the *S* population will be responsible for network stabilization and the paradoxical effect will not be observed in the *P* population.

Overall, these simulations lead to a number of experimental predictions, including the following: (1) that the Pyr ↔ PV loop should be stronger than the Pyr ↔ SST loop; and (2) that strong PV activation should be more effective than SST activation at turning off Up states. Below, we address these two predictions using *ex vivo* cortical circuits.

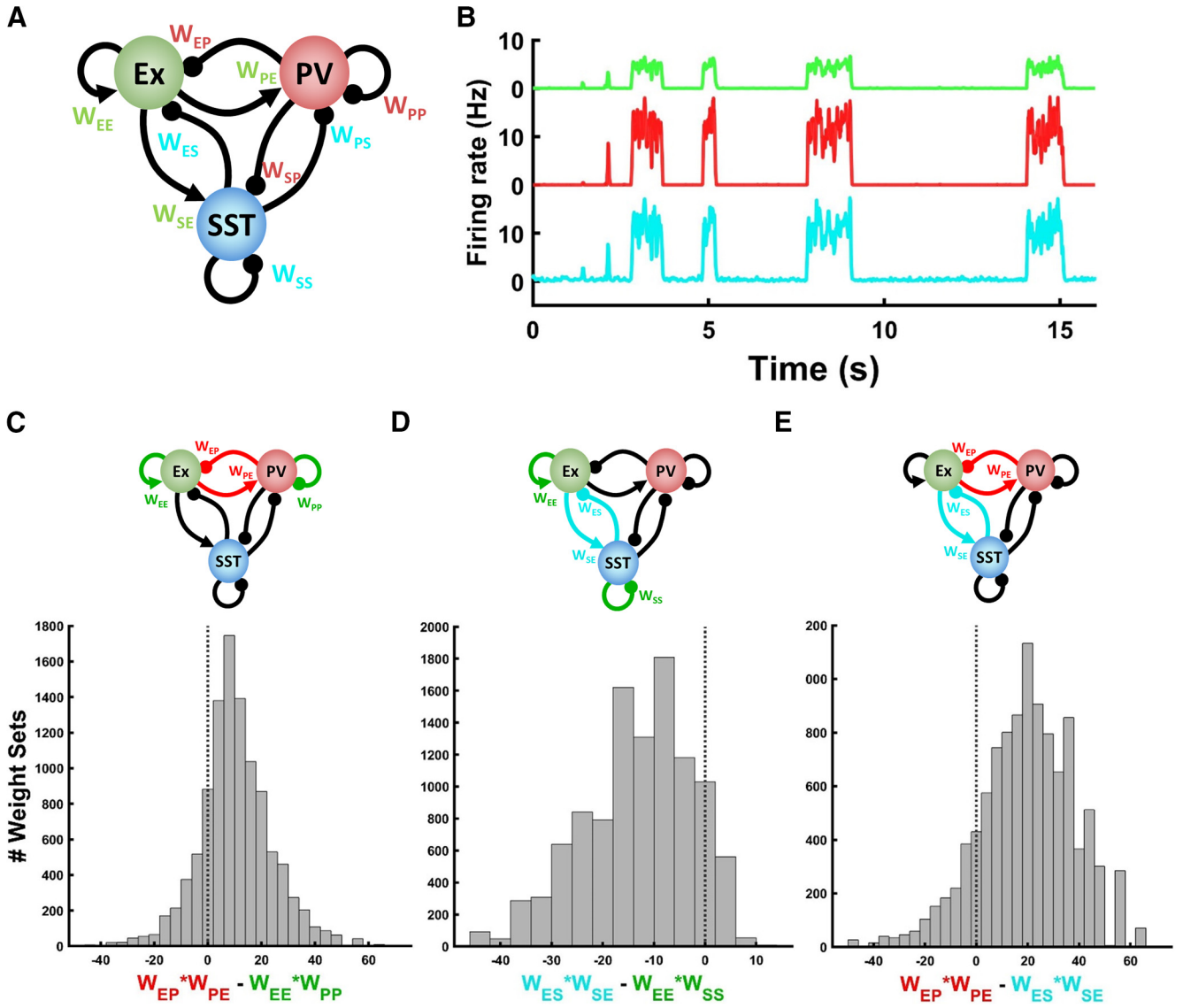

Figure 5. Empirically derived three-population model of Up states. ***A***, Schematic of the fully connected three-population model. Figure conventions are similar to Figure 1*B*. ***B***, Example of Down ↔ Up state transitions in a model with Pyr (top), PV (middle) and SST (bottom) units. The weights were chosen as the set closest to the centroid of the distribution of the fit weight sets. ***C***, Distribution of the fit weight set (i.e., those weight vectors that captured the experimentally observed firing rates) of the inhibitory (red) minus the excitatory (green) loop of the Pyr and PV interaction. ***D***, Distribution of the weights of the inhibitory (cyan) minus the excitatory (green) loop of the Pyr and SST interaction. ***E***, Distribution of the weights of the inhibitory (red) loop of the Pyr–PV minus the inhibitory (cyan) loop of the Pyr–SST interaction.

Testing predictions of the model: paired Pyr-PV and Pyr-SST recordings

To directly examine the predictions of the model, we first performed paired recordings from Pyr–PV and Pyr–SST neuron pairs using *ex vivo* cultures from PV-Cre and PV-SST mice, respectively. As shown in Figure 7, the observed connection probability was consistent with the predictions of the model—note that because the model is population based, the weights reflect both connection probabilities and mean synaptic strengths. Of 53 Pyr–PV and 27 Pyr–SST pairs, we found connections in ~50% and 25% of them, respectively. The Pyr → PV connection probability was 0.31, while the PV → Pyr was 0.23 (Fig. 7*B*). Interestingly, reciprocal connections were more likely than expected from the independent probabilities, indicating that reciprocity is a favored motif (Song et al., 2005). Most of the detected connections involving SST neurons were in the Pyr → SST direction (connection probability = 0.23; Fig. 7*C*). However, we stress that the low probability (0.04) of SST → Pyr connections is likely an underestimation because SST synapses are generally on dendrites and we performed the experiments in current-clamp—making it difficult to detect weak inhibitory connections. The average unitary Pyr → PV amplitude (2.87 ± 0.82 mV) was significantly larger than the unitary Pyr → SST strength (0.70 ± 0.21 mV). The mean PV → Pyr amplitude was (1.93 ± 0.47 mV) larger than the single connected SST → Pyr unitary IPSP amplitude we recorded (0.3 mV). Although these results are limited in their ability to provide quantitative estimates for the model parameters, they confirm the model prediction that the Pyr ↔ PV inhibitory loop is stronger than the Pyr ↔ SST loop in the *ex vivo* system we simulated.

Testing predictions of the model: activation of PV but not SST units turns off Up states

As shown in Figure 6*B*, the model predicts that strong activation of PV neurons during Up states should be more effective at

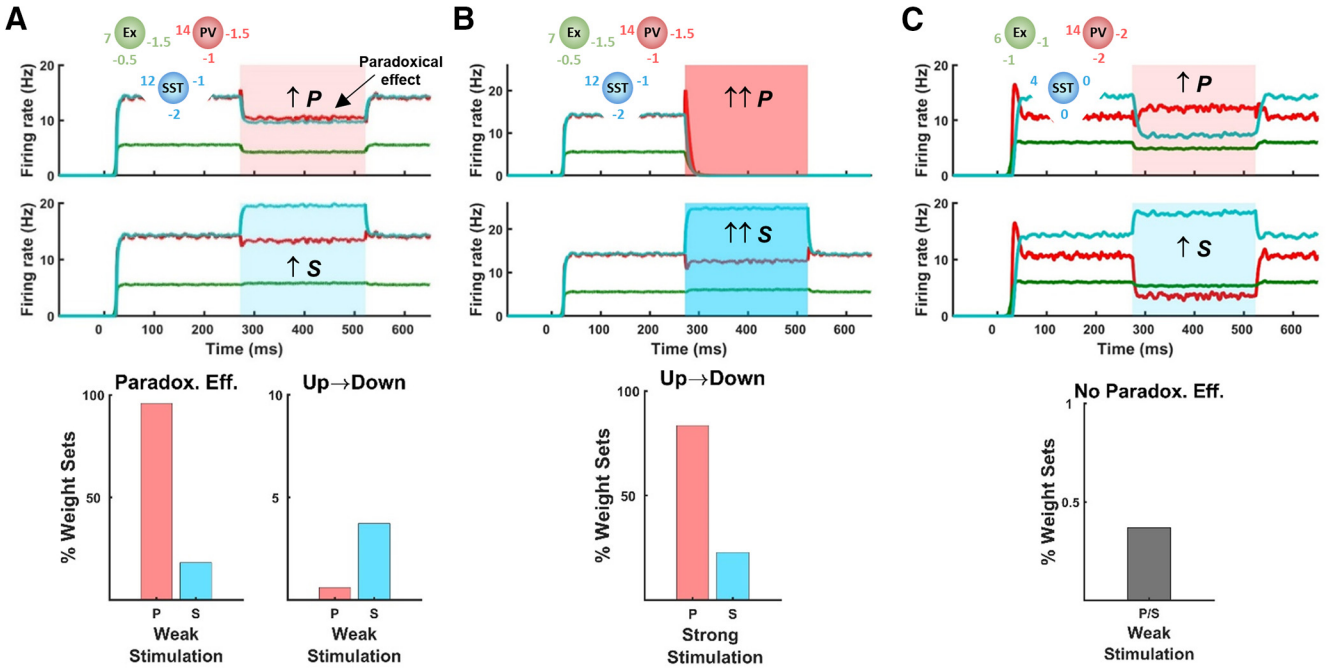

Figure 6. The paradoxical effect in the three-population model. ***A***, Top, Example of weak excitation of the *P* units during an evoked Up state (top, red overlay) showing the paradoxical effect (i.e., despite depolarizing the *P* unit, a decrease in *P* firing rate is observed). In contrast, weak depolarization of the *S* unit (bottom, cyan overlay) did not produce a paradoxical effect in the *S* unit. Bottom, In response to weak activation of *P* units, the paradoxical effect was observed in the *P* units across the vast majority of fit weight sets (left bar of left panel). In contrast, the paradoxical effects were generally not observed in the *S* units in response to weak *S* activation (right bar of left panel). However, *S* activation was more likely to produce Up → Down transitions (right). ***B***, Top, Same as ***C*** with strong activation of *P* (top) and *S* (bottom). Bottom, Strong activation of *P* cells was much more effective at inducing Up → Down transitions across of the validated weights sets. ***C***, Top, Example of a parameter regime in which the paradoxical effect is not observed in either *P* (top) or *S* (bottom) units. Note that in this regime small increases in *P* (*S*) result in relatively larger decreases in *S* (*P*). Bottom, Regimes in which the paradoxical effect is not observed in both *P* and *S* units comprise a very small subset of the total fit weight set.

turning off Up states than the activation of SST neurons. To test this prediction, we expressed ChETA in PV or SST cells in separate *ex vivo* slices and examined whether optogenetic activation of these inhibitory neuron populations produced Up → Down transitions. Toward this end, we recorded from Pyr neurons and triggered a train of light pulses during detected Up-state onsets in slices expressing ChETA in either PV or SST neurons (see Materials and Methods). We used "full-field" light activation to emulate the strong activation of the model (Fig. 6*B*) and to be able to further increase the already high firing rate of inhibitory neurons during Up states (Fig. 2). Optogenetic stimulation of PV and SST neurons effectively increased the inhibitory neuron firing rate even during Up states (Fig. 8). The comparison of light-off and light-on trials during Pyr recordings (Fig. 9) revealed that the activation of PV neurons during Up states was highly effective at inducing Up → Down transitions (mean Up state duration: light off, 1.80 ± 0.36 s; light on, 0.78 ± 0.34 s; $n = 10$, Wilcoxon signed-rank test: $z = 2.80$, $p = 0.005$; Fig. 9*B*). In contrast, SST activation did not produce a significant decrease in Up-state duration (1.76 ± 0.19 s, $n = 21$; 2.12 ± 0.22 s, $n = 21$; $z = -1.09$, $p = 0.28$; Fig. 9*D*). Activation of PV, but not SST, neurons also resulted in a decrease in the membrane potential of Pyr neurons during optical stimulation (Fig. 9*E*,*F*). These results further confirm the prediction of the model, which because Pyr–PV connectivity is stronger than Pyr–SST connectivity, strong activation of PV neurons is more effective at inducing Up → Down transitions. Indeed, these experimental results are in agreement with the prototypical weight set simulations shown in Figure 6*B*, in which strong *P* activation produced an Up → Down transition, and *S* activation had minimal effect on *E* activity.

Discussion

We experimentally characterized the intrinsic input–output function (the *F–I* curve) of three classes of neurons in *ex vivo* organotypic cortical cultures. We incorporated these empirically derived activation functions into a computational model that captures the experimentally observed firing rates, and finally, tested experimental predictions of the model. This integrated *ex vivo* computational approach parallels studies in invertebrate systems (Gingrich and Byrne, 1985; Buonomano et al., 1990; Marder and Calabrese, 1996; Phares et al., 2003; Prinz et al., 2004). Such approaches, however, have been difficult to carry out in neocortical circuits for a number of reasons, including that the network regimes being simulated are often recorded *in vivo*, while the cellular properties are generally obtained from *in vitro* acute slice preparations (and thus under significantly different physiological conditions and network regimes). And in contrast to acute slice studies in which the state of neurons and synapses reflects the homeostatic learning rules shaped by the *in vivo* environment, here we studied *ex vivo* circuits that converged to their homeostatic set points over weeks. Furthermore, all *in vivo* datasets are subject to reciprocal influences from a multitude of brain areas that cannot be incorporated into models. Thus, by studying and modeling an *ex vivo* cortical circuit, it was possible to directly couple the experimental data to the computational model and ensure that the experimental and computational results reflect the properties of local intrinsic circuits.

Differential role of PV and SST neurons in network stabilization

Our findings establish that the empirically derived differences in *F–I* characteristics of PV and SST neurons are sufficient to lead

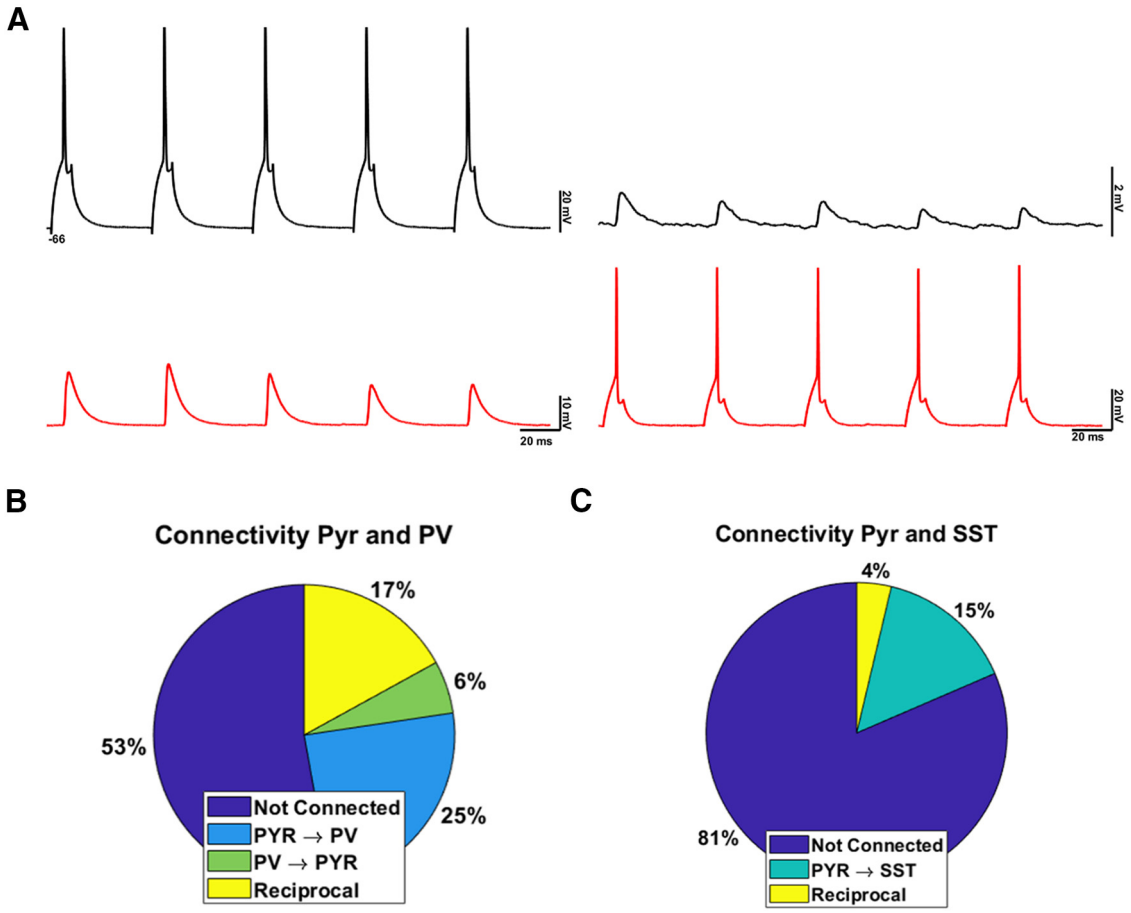

Figure 7. Paired recordings from Pyr–PV and Pyr–SST neuron pairs. ***A***, Simultaneous recording of Pyr and PV neurons. Spikes in the Pyr neuron (top left trace) induce EPSPs in the PV interneuron (bottom left trace), while spikes in PV interneuron (bottom right trace) induced IPSPs in the Pyr neuron (top right trace). ***B***, Pie chart of connectivity of Pyr–PV pairs. ***C***, Same as ***B*** but for Pyr–SST neuron pairs.

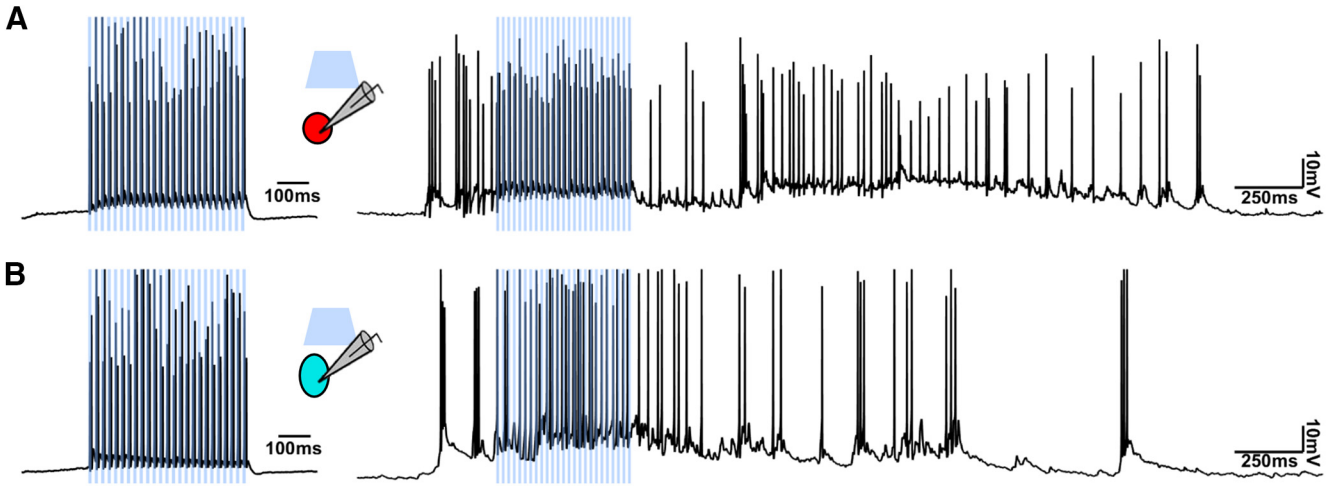

Figure 8. Examples of optical activation of inhibitory neurons. ***A***, Example of an optical induced increase in the firing rate of a PV ChETA-positive neuron during a Down state (left) and an Up state (right). ***B***, Same as ***A*** but for an SST neuron.

to a pronounced differential contribution of these neuron classes to network dynamics. The threshold and gain of PV neurons were higher than those of SST neurons. This signature is critical to the stabilization of Up states for the following two reasons: (1) the increased threshold means that the excitatory neurons can engage in positive feedback at very low firing rates before triggering inhibition; and (2) once the inhibitory neurons reach threshold, they can quickly overtake the activity in the excitatory neurons because of their larger gain (Jercog et al., 2017), thus stabilizing the network. Interestingly, while the differential gain between PV and SST neurons has not been carefully contrasted in the past, the threshold difference in PV and SST neurons is a

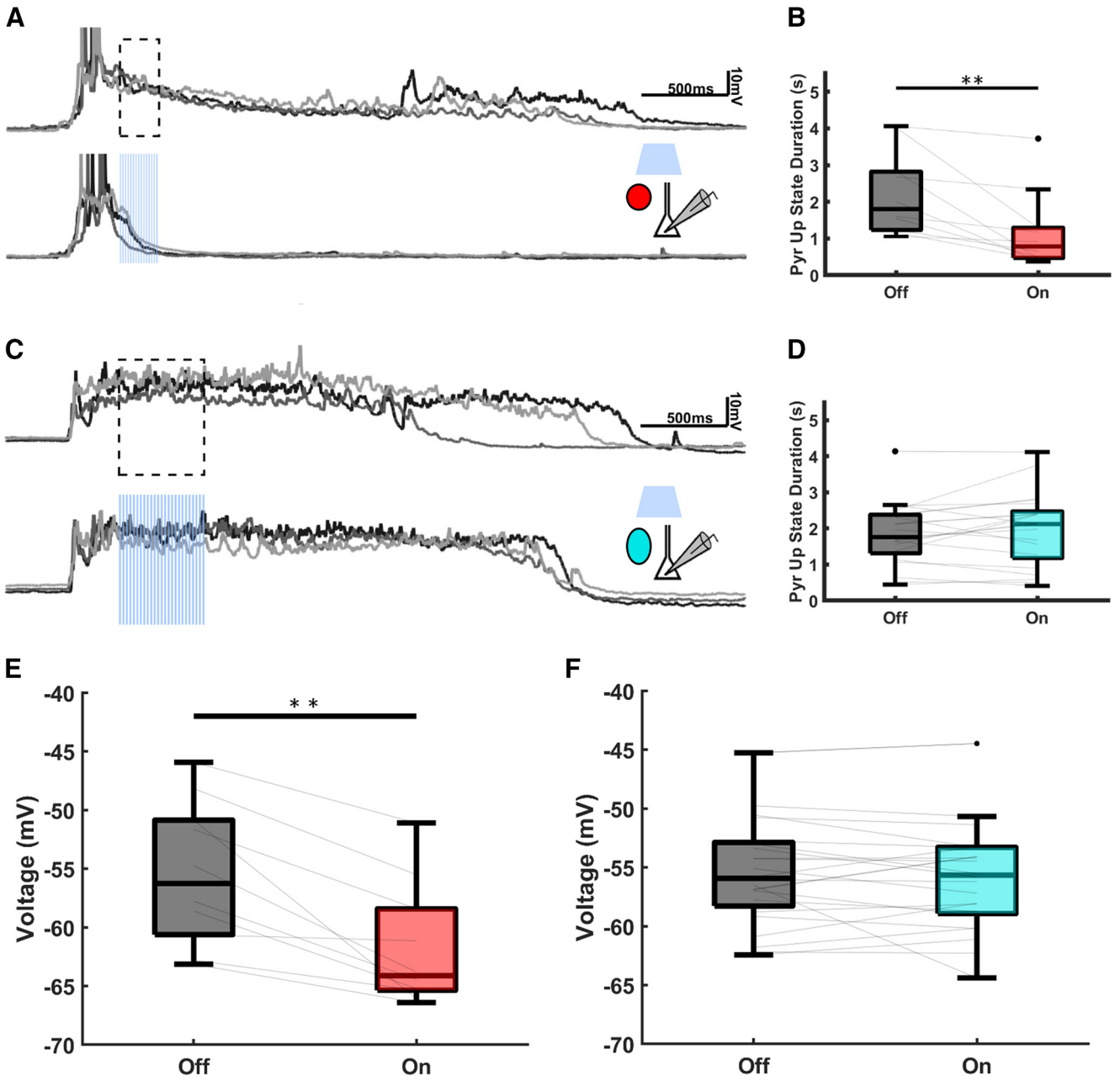

Figure 9. Differential effects of PV and SST interneurons on turning off Up states. ***A***, PV light activation resulted in shorter Up states as depicted by individual traces (bottom, gray) and the mean Up-state trace (bottom, black) compared with Up states in which light was not presented (top traces). ***B***, Median Pyr Up-state duration was significantly shorter when the light was delivered during Up states compared with Up states that did not receive light stimulation. ***C***, Same as ***A*** but for SST neurons. Up states that were presented with light are not different from unstimulated Up states. ***D***, SST activation during Up states resulted in similar Up-state durations compared with unstimulated Up states. ***E***, The median membrane voltage of Pyr neurons was significantly reduced during optical stimulation of PV neurons. ***F***, The median voltage of Pyr neurons was not significant during optical stimulation of SST neurons.

defining distinction between them (e.g., so-called low-threshold inhibitory neurons correspond to SST neurons; Gupta et al., 2000; Rudy et al., 2011; Cardin, 2018). Thus, our results emphasize that a critical functional difference between PV and SST neurons is that both the threshold and gain of the *F–I* function of PV neurons are larger than those of SST neurons.

It is generally accepted that the observed diversity of inhibitory neurons is a reflection of the fact that cortical computations require inhibition to fulfill multiple functional roles (Wang et al., 2004; Pfeffer et al., 2013; Natan et al., 2015). However, while the differential contribution of these neurons has focused primarily on their synaptic and connectivity properties, our results suggest a critical role of the differential input–output function of inhibitory neuron subclasses in cortical dynamics. Furthermore, the importance of the difference in the intrinsic excitability properties of PV and SST neurons is consistent with the importance of intrinsic excitability in neural computations (Marder and Calabrese, 1996; Josselyn and Tonegawa, 2020). However, an open question pertains to the degree to which the input–output functions of PV and SST neurons are plastic. While it seems likely that the threshold and gain parameters of these neural populations undergo some forms of intrinsic plasticity (Daoudal and Debanne, 2003; Zhang and Linden, 2003; Debanne et al., 2019), we would hypothesize that fundamental properties reported here (i.e., $\theta_P > \theta_S$ and $g_P > g_S$) reflect fundamental and hard-wired differences within these populations.

Because the experimental data were collected in *ex vivo* cortical circuits, our results provide insights into the unsupervised learning rules governing the emergence of Up states. Specifically, Up states seem to reflect states that cortical circuits actively seek out through homeostatic mechanisms. For example, while cortical cultures are initially silent, spontaneous and evoked Up states emerge over the course of *ex vivo* development (van Pelt et al., 2005; Johnson and Buonomano, 2007; Motanis and Buonomano, 2015, 2020). This suggests that a set of learning rules in place *ex vivo* drive networks toward Up–Down state transitions similar to those observed *in vivo* and in acute slices (Sanchez-Vives and McCormick, 2000). Given the critical stabilizing effect of PV neurons, our results suggest that these learning rules may operate primarily on PV neurons.

The computational model predicted that the strength of the Pyr ↔ PV inhibitory loop is significantly stronger than the Pyr ↔ SST loop. Paired recordings and optogenetic experiments validated these predictions. Previous studies have generally reported robust connectivity (>50%) between PV → Pyr and SST → Pyr neurons (Silberberg and Markram, 2007; Fino and Yuste, 2011; Packer and Yuste, 2011; Pfeffer et al., 2013; Pala and Petersen, 2015), but, consistent with our experimental and computational results, the Pyr ↔ PV loop seems to be stronger than the Pyr ↔ SST loop (e.g., the connection probability from Pyr → PV has been reported to be higher than the Pyr → SST loop; Pala and Petersen, 2015) and the PV → Pyr connections to be stronger than the SST → Pyr connections (Pfeffer et al., 2013).

The above results, however, do not imply that *in vivo* SST neurons do not play a significant role in Up-state dynamics. While it remains an open question whether SST neurons are necessary for Up states, it is well established that they are highly active during Up states, and that manipulation of SST activity can alter Up-state dynamics. For example, an *in vivo* study reported that both PV and SST activation could terminate Up states (Zucca et al., 2017), and SST neuron activation during Up states has also been shown to increase Pyr firing in acute slices (Neske and Connors, 2016). Additionally, it has been shown that SST activity during Up states modulates the strength of Pyr → Pyr connections (Urban-Ciecko et al., 2015). Interestingly, however, SST neurons have been reported to be decorrelated with Pyr neuron activity in response to sensory stimuli, active during locomotion, and to exhibit high levels of spontaneous firing *in vivo* and *in vitro* (Gentet et al., 2012; Polack et al., 2013; Urban-Ciecko et al., 2015; Urban-Ciecko and Barth, 2016; Yaeger et al., 2019). Overall, these studies suggest that there is an as yet not fully understood state-dependent modulation of the coupling between SST and Pyr activity. Here we observed a correlation between SST and Pyr activity, but did not observe any clear effect of SST activity manipulation on Up states. But, given the ability of cortical circuits to adapt to a wide range of natural and pathologic regimes, it is likely that different inhibitory neurons play different roles in different contexts. Our results suggest that under highly controlled conditions and in the absence of external input from other brain areas, cortical microcircuits converge to regimes where PV neurons are primarily responsible for inhibition stabilization and emergent dynamic regimes. Thus, we predict that while PV neurons are necessary for Up states, SST neurons may modulate Up-state properties. Furthermore, our results suggest that future research on the learning rules governing network Up-state dynamics should focus primarily on plasticity of the Pyr ↔ PV loop.

It is also relevant to point out that the model used here is a highly simplified approximation of biological networks. In particular the gain, time constants, and weights of neurons in actual circuits are not necessarily the same during low- and high-firing rate regimes (Dobrunz and Stevens, 1999; Rauch et al., 2003; La Camera et al., 2006), and we have not taken into account the differential adaptation of different inhibitory neuron subtypes (Tateno et al., 2004). Thus, it is possible that some of the differences between experimental studies, and between the experiments and models, could be related to state-dependent changes in variables held constant in our models, including the *F–I* gain and short-term synaptic plasticity of synaptic weights.

The paradoxical effect and predictions

The standard two-population model of Up states predicts the presence of a paradoxical effect, in which external depolarization of the inhibitory neuron population during an Up state will counterintuitively decrease the firing rate of inhibitory neurons. Testing this prediction has been experimentally challenging for a number of reasons, including the need to record and carefully control the levels of external input to a specific inhibitory neuron population during Up states (Sanzeni et al., 2020). Some experiments have reported signatures consistent with the paradoxical effect (Kato et al., 2017; Moore et al., 2018; Sanzeni et al., 2020), while others have not (Xu et al., 2013; Gutnisky et al., 2017). Recent computational studies have established that the paradoxical effect is not obligatory in models that include multiple types of inhibitory neurons (Litwin-Kumar et al., 2016; Mahrach et al., 2020; Sanzeni et al., 2020). Consistent with these findings our analysis shows that whether the paradoxical effect is present or not in PV neurons depends on the relationship of the excitatory ($W_{EE} * W_{SS}$) and inhibitory loop ($W_{ES} * W_{SE}$) between the Pyr and SST populations. It is relevant to note that, in contrast to previous studies, here the difference between PV and SST populations was based on their intrinsic properties rather than differences in the connectivity matrices.

Our numerical results revealed that in the vast majority of cases the paradoxical effect was observed in either the PV or SST population (Fig. 6); however, there is a very narrow regime in which neither population of inhibitory neurons revealed a paradoxical effect. Based on our numerical simulations, we predict that the paradoxical effect should be observed in PV neurons, although it is possible that some failures to observe the paradoxical effect in PV neurons could reflect situations in which the SST neurons are driving network stabilization, in which case they should exhibit the paradoxical effect. One must also consider the possibility that experimental failures to observe the paradoxical effect may be because the standard computational models of Up states, including ours, lack critical biological ingredients. For example, most models do not explicitly distinguish between the contribution of $GABA_A$ and $GABA_B$ receptor-mediated inhibition, yet $GABA_B$-mediated inhibition powerfully regulates Up states (Mann et al., 2009; Urban-Ciecko et al., 2015). Future work will attempt to explicitly address the paradoxical effect in both PV and SST neurons in our preparation and the potential contribution of other mechanisms to Up-state dynamics.

Conclusions

Using an *ex vivo* preparation, it was possible to use empirically derived fits of the *F–I* functions of PV and SST neurons to create a model of Up-state dynamics and fit the weights of the model to the empirically derived Up-state firing rates. This approach allowed for a direct link between the experimental and computational components of the study. The results establish that the differential intrinsic properties of the PV and SST neurons, specifically the higher threshold and gain of the PV neurons, are in and of themselves sufficient to drive a distinct role of these

inhibitory neurons classes in Up-state dynamics. While previous work has focused on the differential synaptic and connectivity patterns of PV and SST to cortical function, the current results emphasize that the differential threshold and gain of the *F–I* function of these inhibitory subclasses may underlie their distinct functional roles.

References

Adesnik H, Bruns W, Taniguchi H, Huang ZJ, Scanziani M (2012) A neural circuit for spatial summation in visual cortex. Nature 490:226–231.

Bartram J, Kahn MC, Tuohy S, Paulsen O, Wilson T, Mann EO (2017) Cortical Up states induce the selective weakening of subthreshold synaptic inputs. Nat Commun 8:665.

Beltramo R, D'Urso G, Dal Maschio M, Farisello P, Bovetti S, Clovis Y, Lassi G, Tucci V, De Pietri Tonelli D, Fellin T (2013) Layer-specific excitatory circuits differentially control recurrent network dynamics in the neocortex. Nat Neurosci 16:227–234.

Brunel N (2000) Dynamics of sparsely connected networks of excitatory and inhibitory spiking neurons. J Comput Neurosci 8:183–208.

Buonomano DV (2003) Timing of neural responses in cortical organotypic slices. Proc Natl Acad Sci U S A 100:4897–4902.

Buonomano DV, Maass W (2009) State-dependent computations: spatiotemporal processing in cortical networks. Nat Rev Neurosci 10:113–125.

Buonomano DV, Baxter DA, Byrne JH (1990) Small networks of empirically derived adaptive elements simulate some higher-order features of classical conditioning. Neural Netw 3:507–523.

Cardin JA (2018) Inhibitory interneurons regulate temporal precision and correlations in cortical circuits. Trends Neurosci 41:689–700.

Carnevale F, de Lafuente V, Romo R, Barak O, Parga N (2015) Dynamic control of response criterion in premotor cortex during perceptual detection under temporal uncertainty. Neuron 86:1067–1077.

Carrillo-Reid L, Miller J-eK, Hamm JP, Jackson J, Yuste R (2015) Endogenous sequential cortical activity evoked by visual stimuli. J Neurosci 35:8813–8828.

Chaisangmongkon W, Swaminathan SK, Freedman DJ, Wang X-J (2017) Computing by robust transience: how the fronto-parietal network performs sequential, category-based decisions. Neuron 93:1504–1517.e4.

Connors BW (1984) Initiation of synchronized neuronal bursting in neocortex. Nature 310:685–687.

Constantinople CM, Bruno RM (2011) Effects and mechanisms of wakefulness on local cortical networks. Neuron 69:1061–1068.

Crochet S, Petersen CCH (2006) Correlating whisker behavior with membrane potential in barrel cortex of awake mice. Nat Neurosci 9:608–610.

Dao Duc K, Parutto P, Chen X, Epsztein J, Konnerth A, Holcman D (2015) Synaptic dynamics and neuronal network connectivity are reflected in the distribution of times in up states. Front Comput Neurosci 9:96.

Daoudal G, Debanne D (2003) Long-term plasticity of intrinsic excitability: learning rules and mechanisms. Learn Mem 10:456–465.

Debanne D, Gähwiler BH, Thompson SM (1994) Asynchronous pre- and postsynaptic activity induces associative long-term depression in area CA1 of the rat hippocampus in vitro. Proc Natl Acad Sci U S A 91:1148–1152.

Debanne D, Inglebert Y, Russier M (2019) Plasticity of intrinsic neuronal excitability. Curr Opin Neurobiol 54:73–82.

Dechery JB, MacLean JN (2017) Emergent cortical circuit dynamics contain dense, interwoven ensembles of spike sequences. J Neurophysiol 118:1914–1925.

Destexhe A, Hughes SW, Rudolph M, Crunelli V (2007) Are corticothalamic "up" states fragments of wakefulness? Trends Neurosci 30:334–342.

Diekelmann S, Born J (2010) The memory function of sleep. Nat Rev Neurosci 11:114–126.

Dobrunz LE, Stevens CF (1999) Response of hippocampal synapses to natural stimulation patterns. Neuron 22:157–166.

Douglas RJ, Martin KAC (2007) Mapping the matrix: the ways of neocortex. Neuron 56:226–238.

Esteban JA, Shi S-H, Wilson C, Nuriya M, Huganir RL, Malinow R (2003) PKA phosphorylation of AMPA receptor subunits controls synaptic trafficking underlying plasticity. Nat Neurosci 6:136–143.

Fanselow EE, Connors BW (2010) The roles of somatostatin-expressing (GIN) and fast-spiking inhibitory interneurons in up-down states of mouse neocortex. J Neurophysiol 104:596–606.

Fino E, Yuste R (2011) Dense inhibitory connectivity in neocortex. Neuron 69:1188–1203.

Funahashi S, Bruce CJ, Goldman-Rakic PS (1993) Dorsolateral prefrontal lesions and oculomotor delayed-response performance: evidence for mnemonic "scotomas". J Neurosci 13:1479–1497.

Gentet LJ, Kremer Y, Taniguchi H, Huang ZJ, Staiger JF, Petersen CCH (2012) Unique functional properties of somatostatin-expressing GABAergic neurons in mouse barrel cortex. Nat Neurosci 15:607–612.

Gingrich KJ, Byrne JH (1985) Simulation of synaptic depression, posttetanic potentiation, and presynaptic facilitation of synaptic potentials from sensory neurons mediating gill-withdrawal reflex in Aplysia. J Neurophysiol 53:652–669.

Goold CP, Nicoll RA (2010) Single-cell optogenetic excitation drives homeostatic synaptic depression. Neuron 68:512–528.

Guo ZV, Inagaki HK, Daie K, Druckmann S, Gerfen CR, Svoboda K (2017) Maintenance of persistent activity in a frontal thalamocortical loop. Nature 545:181–186.

Gupta A, Wang Y, Markram H (2000) Organizing principles for a diversity of GABAergic interneurons and synapses in the neocortex. Science 287:273–278.

Gutnisky DA, Yu J, Hires SA, To M-S, Bale MR, Svoboda K, Golomb D (2017) Mechanisms underlying a thalamocortical transformation during active tactile sensation. PLoS Comput Biol 13:e1005576.

Haider B, Duque A, Hasenstaub AR, Yu Y, McCormick DA (2007) Enhancement of visual responsiveness by spontaneous local network activity in vivo. J Neurophysiol 97:4186–4202.

Hayashi Y, Shi SH, Esteban JA, Piccini A, Poncer JC, Malinow R (2000) Driving AMPA receptors into synapses by LTP and CaMKII: requirement for GluR1 and PDZ domain interaction. Science 287:2262–2267.

Hebb DO (1949) Organization of behavior. New York: Wiley.

Holcman D, Tsodyks M (2006) The emergence of up and down states in cortical networks. PLoS Comput Biol 2:e23.

Hopfield JJ (1982) Neural networks and physical systems with emergent collective computational abilities. Proc Natl Acad Sci U S A 79:2554–2558.

Hromádka T, Zador AM, DeWeese MR (2013) Up states are rare in awake auditory cortex. J Neurophysiol 109:1989–1995.

Huertas MA, Hussain Shuler MG, Shouval HZ (2015) A simple network architecture accounts for diverse reward time responses in primary visual cortex. J Neurosci 35:12659–12672.

Inagaki HK, Fontolan L, Romani S, Svoboda K (2019) Discrete attractor dynamics underlies persistent activity in the frontal cortex. Nature 566:212–217.

Jercog D, Roxin A, Barthó P, Luczak A, Compte A, de la Rocha J (2017) UP-DOWN cortical dynamics reflect state transitions in a bistable network. eLife 6:e22425.

Johnson HA, Buonomano DV (2007) Development and plasticity of spontaneous activity and up states in cortical organotypic slices. J Neurosci 27:5915–5925.

Josselyn SA, Tonegawa S (2020) Memory engrams: recalling the past and imagining the future. Science 367:eaaw4325.

Kato HK, Asinof SK, Isaacson JS (2017) Network-level control of frequency tuning in auditory cortex. Neuron 95:412–423.e4.

Kerr JN, Plenz D (2004) Action potential timing determines dendritic calcium during striatal up-states. J Neurosci 24:877–885.

Krabbe S, Paradiso E, d'Aquin S, Bitterman Y, Courtin J, Xu C, Yonehara K, Markovic M, Müller C, Eichlisberger T, Gründemann J, Ferraguti F, Lüthi A (2019) Adaptive disinhibitory gating by VIP interneurons permits associative learning. Nat Neurosci 22:1834–1843.

Kroener S, Chandler LJ, Phillips PEM, Seamans JK (2009) Dopamine modulates persistent synaptic activity and enhances the signal-to-noise ratio in the prefrontal cortex. PLoS One 4:e6507.

Kuhlman SJ, Olivas ND, Tring E, Ikrar T, Xu X, Trachtenberg JT (2013) A disinhibitory microcircuit initiates critical-period plasticity in the visual cortex. Nature 501:543–546.

La Camera G, Rauch A, Thurbon D, Lüscher H-R, Senn W, Fusi S (2006) Multiple time scales of temporal response in pyramidal and fast spiking cortical neurons. J Neurophysiol 96:3448–3464.

Litwin-Kumar A, Rosenbaum R, Doiron B (2016) Inhibitory stabilization and visual coding in cortical circuits with multiple interneuron subtypes. J Neurophysiol 115:1399–1409.

Lőrincz ML, Gunner D, Bao Y, Connelly WM, Isaac JTR, Hughes SW, Crunelli V (2015) A distinct class of slow (~0.2–2 Hz) intrinsically bursting layer 5 pyramidal neurons determines UP/DOWN state dynamics in the neocortex. J Neurosci 35:5442–5458.

Mahrach A, Chen G, Li N, van Vreeswijk C, Hansel D (2020) Mechanisms underlying the response of mouse cortical networks to optogenetic manipulation. eLife 9:e49967.

Mann EO, Kohl MM, Paulsen O (2009) Distinct roles of $GABA_A$ and $GABA_B$ receptors in balancing and terminating persistent cortical activity. J Neurosci 29:7513–7518.

Marder E, Calabrese RL (1996) Principles of rhythmic motor pattern generation. Physiol Rev 76:687–717.

Marshall L, Helgadóttir H, Mölle M, Born J (2006) Boosting slow oscillations during sleep potentiates memory. Nature 444:610–613.

Mauk MD, Buonomano DV (2004) The neural basis of temporal processing. Annu Rev Neurosci 27:307–340.

Moore AK, Weible AP, Balmer TS, Trussell LO, Wehr M (2018) Rapid rebalancing of excitation and inhibition by cortical circuitry. Neuron 97:1341–1355.e6.

Motanis H, Buonomano DV (2015) Delayed in vitro development of up states but normal network plasticity in fragile X circuits. Eur J Neurosci 42:2312–2321.

Motanis H, Buonomano D (2020) Decreased reproducibility and abnormal experience-dependent plasticity of network dynamics in Fragile X circuits. Sci Rep 10:14535.

Namboodiri V, Huertas M, Monk K, Shouval H, Shuler M (2015) Visually cued action timing in the primary visual cortex. Neuron 86:319–330.

Natan RG, Briguglio JJ, Mwilambwe-Tshilobo L, Jones SI, Aizenberg M, Goldberg EM, Geffen MN (2015) Complementary control of sensory adaptation by two types of cortical interneurons. eLife 4:e09868.

Natan RG, Rao W, Geffen MN (2017) Cortical interneurons differentially shape frequency tuning following adaptation. Cell Rep 21:878–890.

Neske GT, Connors BW (2016) Distinct roles of SOM and VIP interneurons during cortical up states. Front Neural Circuits 10:52.

Neske GT, Patrick SL, Connors BW (2015) Contributions of diverse excitatory and inhibitory neurons to recurrent network activity in cerebral cortex. J Neurosci 35:1089–1105.

Ozeki H, Finn IM, Schaffer ES, Miller KD, Ferster D (2009) Inhibitory stabilization of the cortical network underlies visual surround suppression. Neuron 62:578–592.

Packer AM, Yuste R (2011) Dense, unspecific connectivity of neocortical parvalbumin-positive interneurons: a canonical microcircuit for inhibition? J Neurosci 31:13260–13271.

Pala A, Petersen CCH (2015) In vivo measurement of cell-type-specific synaptic connectivity and synaptic transmission in layer 2/3 mouse barrel cortex. Neuron 85:68–75.

Pfeffer CK, Xue M, He M, Huang ZJ, Scanziani M (2013) Inhibition of inhibition in visual cortex: the logic of connections between molecularly distinct interneurons. Nat Neurosci 16:1068–1076.

Phares GA, Antzoulatos EG, Baxter DA, Byrne JH (2003) Burst-induced synaptic depression and its modulation contribute to information transfer at *Aplysia* sensorimotor synapses: empirical and computational analyses. J Neurosci 23:8392–8401.

Pi HJ, Hangya B, Kvitsiani D, Sanders JI, Huang ZJ, Kepecs A (2013) Cortical interneurons that specialize in disinhibitory control. Nature 503:521–524.

Plenz D, Kitai ST (1998) Up and down states in striatal medium spiny neurons simultaneously recorded with spontaneous activity in fast-spiking interneurons studied in cortex-striatum-substantia nigra organotypic cultures. J Neurosci 18:266–283.

Polack P-O, Friedman J, Golshani P (2013) Cellular mechanisms of brain state–dependent gain modulation in visual cortex. Nat Neurosci 16:1331–1339.

Prince DA, Tseng GF (1993) Epileptogenesis in chronically injured cortex: in vitro studies. J Neurophysiol 69:1276–1291.

Prinz AA, Bucher D, Marder E (2004) Similar network activity from disparate circuit parameters. Nat Neurosci 7:1345–1352.

Quintana J, Fuster JM (1992) Mnemonic and predictive functions of cortical neurons in a memory task. Neuroreport 3:721–724.

Rabinovich M, Huerta R, Laurent G (2008) Transient dynamics for neural processing. Science 321:48–50.

Rauch A, Camera GL, Lüscher H-R, Senn W, Fusi S (2003) Neocortical pyramidal cells respond as integrate-and-fire neurons to in vivo–like input currents. J Neurophysiol 90:1598–1612.

Renart A, de la Rocha J, Bartho P, Hollender L, Parga N, Reyes A, Harris KD (2010) The asynchronous state in cortical circuits. Science 327:587–590.

Rubin DB, Van Hooser SD, Miller KD (2015) The stabilized supralinear network: a unifying circuit motif underlying multi-input integration in sensory cortex. Neuron 85:402–417.

Rudy B, Fishell G, Lee S, Hjerling-Leffler J (2011) Three groups of interneurons account for nearly 100% of neocortical GABAergic neurons. Dev Neurobiol 71:45–61.

Sadovsky AJ, MacLean JN (2014) Mouse visual neocortex supports multiple stereotyped patterns of microcircuit activity. J Neurosci 34:7769–7777.

Sanchez-Vives MV, McCormick DA (2000) Cellular and network mechanisms of rhythmic recurrent activity in neocortex. Nat Neurosci 3:1027–1034.

Sanzeni A, Akitake B, Goldbach HC, Leedy CE, Brunel N, Histed MH (2020) Inhibition stabilization is a widespread property of cortical networks. eLife 9:e54875.

Seamans JK, Nogueira L, Lavin A (2003) Synaptic basis of persistent activity in prefrontal cortex in vivo and in organotypic cultures. Cereb Cortex 13:1242–1250.

Shriki O, Hansel D, Sompolinsky H (2003) Rate models for conductance-based cortical neuronal networks. Neural Comput 15:1809–1841.

Shu Y, Hasenstaub A, McCormick DA (2003) Turning on and off recurrent balanced cortical activity. Nature 423:288–293.

Shuler MG, Bear MF (2006) Reward timing in the primary visual cortex. Science 311:1606–1609.

Silberberg G, Markram H (2007) Disynaptic inhibition between neocortical pyramidal cells mediated by martinotti cells. Neuron 53:735–746.

Sippy T, Yuste R (2013) Decorrelating action of inhibition in neocortical networks. J Neurosci 33:9813–9830.

Sirota A, Buzsáki G (2005) Interaction between neocortical and hippocampal networks via slow oscillations. Thalamus Relat Syst 3:245–259.

Song S, Sjostrom PJ, Reigl M, Nelson Chklovskii DB (2005) Highly nonrandom feature of synaptic connectivity in local cortical circuits. PLOS Biology 3:508–518.

Steriade M, McCormick D, Sejnowski T (1993) Thalamocortical oscillations in the sleeping and aroused brain. Science 262:679–685.

Stoppini L, Buchs PA, Muller D (1991) A simple method for organotypic cultures of nervous tissue. J Neurosci Methods 37:173–182.

Tan AYY, Chen Y, Scholl B, Seidemann E, Priebe NJ (2014) Sensory stimulation shifts visual cortex from synchronous to asynchronous states. Nature 509:226–229.

Tartaglia EM, Brunel N (2017) Bistability and up/down state alternations in inhibition-dominated randomly connected networks of LIF neurons. Sci Rep 7:11916.

Tateno T, Harsch A, Robinson HPC (2004) Threshold firing frequency–current relationships of neurons in rat somatosensory cortex: type 1 and type 2 dynamics. J Neurophysiol 92:2283–2294.

Timofeev I, Grenier F, Bazhenov M, Sejnowski TJ, Steriade M (2000) Origin of slow cortical oscillations in deafferented cortical slabs. Cereb Cortex 10:1185–1199.

Timofeev I, Grenier F, Steriade M (2004) Contribution of intrinsic neuronal factors in the generation of cortically driven electrographic seizures. J Neurophysiol 92:1133–1143.

Tononi G, Cirelli C (2003) Sleep and synaptic homeostasis: a hypothesis. Brain Res Bull 62:143–150.

Tsodyks MV, Skaggs WE, Sejnowski TJ, McNaughton BL (1997) Paradoxical effects of external modulation of inhibitory interneurons. J Neurosci 17:4382–4388.

Urban-Ciecko J, Barth AL (2016) Somatostatin-expressing neurons in cortical networks. Nat Rev Neurosci 17:401–409.

Urban-Ciecko J, Fanselow EE, Barth AL (2015) Neocortical somatostatin neurons reversibly silence excitatory transmission via GABAb receptors. Curr Biol 25:722–731.

van Pelt J, Vajda I, Wolters PS, Corner MA, Ramakers GJ (2005) Dynamics and plasticity in developing neuronal networks in vitro. Prog Brain Res 147:173–188.

Vyazovskiy VV, Cirelli C, Pfister-Genskow M, Faraguna U, Tononi G (2008) Molecular and electrophysiological evidence for net synaptic potentiation in wake and depression in sleep. Nat Neurosci 11:200–208.

Wang X-J (2001) Synaptic reverberation underlying mnemonic persistent activity. Trends Neurosci 24:455–463.

Wang X-J, Tegnér J, Constantinidis C, Goldman-Rakic PS (2004) Division of labor among distinct subtypes of inhibitory neurons in a cortical microcircuit of working memory. Proc Natl Acad Sci U S A 101:1368–1373.

Xu H, Jeong H-Y, Tremblay R, Rudy B (2013) Neocortical somatostatin-expressing GABAergic interneurons disinhibit the thalamorecipient layer 4. Neuron 77:155–167.

Yaeger CE, Ringach DL, Trachtenberg JT (2019) Neuromodulatory control of localized dendritic spiking in critical period cortex. Nature 567:100–104.

Yamada A, Uesaka N, Hayano Y, Tabata T, Kano M, Yamamoto N (2010) Role of pre- and postsynaptic activity in thalamocortical axon branching. Proc Natl Acad Sci U S A 107:7562–7567.

Zhang W, Linden DJ (2003) The other side of the engram: experience-driven changes in neuronal intrinsic excitability. Nat Rev Neurosci 4:885–900.

Zucca S, D'Urso G, Pasquale V, Vecchia D, Pica G, Bovetti S, Moretti C, Varani S, Molano-Mazón M, Chiappalone M, Panzeri S, Fellin T (2017) An inhibitory gate for state transition in cortex. eLife 6:e26177.